Scaling at the Mott–Hubbard metal–insulator transition in yttrium hydride

2003 J. Phys.: Condens. Matter 15 1405

(http://iopscience.iop.org/0953-8984/15/9/304)

INSTITUTE OF PHYSICS PUBLISHING JOURNAL OF PHYSICS: CONDENSED MATTER

J. Phys.: Condens. Matter **15** (2003) 1405–1413 PII: S0953-8984(03)58288-1

Scaling at the Mott–Hubbard metal–insulator transition in yttrium hydride

A F Th Hoekstra[1,2], **A S Roy**[2] **and T F Rosenbaum**[2]

[1] Kamerlingh Onnes Laboratory, Leiden University, Leiden, NL-2300RA, The Netherlands
[2] The James Franck Institute and Department of Physics, The University of Chicago, Chicago, IL 60637, USA

Received 14 January 2003
Published 24 February 2003
Online at stacks.iop.org/JPhysCM/15/1405

Abstract

A single yttrium hydride thin film is conveniently driven through the $T = 0$ metal–insulator transition by fine-tuning the charge carrier density n via persistent photoconductivity at low temperature. Simultaneously, electrical conductivity and Hall measurements are performed for temperatures T down to 350 mK and magnetic fields up to 14 T. A scaling analysis is applied and critical exponents, resolved separately on the metallic and insulating sides of the critical region, are determined consistently. We introduce corrections to scaling to invoke collapse of the data onto a single master curve over an extended region of the (n, T) phase diagram.

1. Introduction

The spectacular, reversible optical and electrical properties of thin-film rare-earth hydrides (REH_x) for hydrogen content $2 < x < 3$ at room temperature have been assumed from their discovery [1] to reflect a continuous metal–insulator (MI) transition at the absolute zero of temperature. Through high-resolution studies at sub-kelvin temperatures, we show [2, 3] that the characteristic response of thin-film YH_x, the prototype of these 'switchable mirrors', is indeed connected to a continuous quantum phase transition—a fundamental change of the ground state of the system as a function of a tuning parameter other than temperature T [4]. We are able to drive a single sample through the $T = 0$ MI transition by systematically tuning its charge carrier density n via alternating use of hydrogenation at room temperature (RT) and persistent photoconductivity (PPC) at low T [5], where hydrogen diffusion is negligible. The transition is monitored by measuring the electrical conductivity σ for T down to 0.3 K in magnetic fields up to 14 T. The charge carrier density n is accurately determined from Hall measurements, under the assumption of a single-band model (see [2] and [6] for further details of the sample and experimental methods). The resulting $\sigma(n, T)$ data are consistently interleaved, indicating a common mechanism of charge carrier doping for both tuning methods, although only n changes with PPC, while both x and n vary with hydrogenation. The use of

0953-8984/03/091405+09$30.00

thin-film REHx is crucial to the success of the experiment: bulk samples pulverize due to the large volume expansion that accompanies hydrogenation, while clamping of the substrate inhibits powdering of thin films. Comparison of $\sigma(T)$ for polycrystalline and epitaxial films with $\sigma(T)$ for bulk samples of YH_x indicates that the effect of stresses from (thermal) mismatch with the substrate is negligible.

The existence of various transitions *as a function of* T for REH_x powder samples *at fixed* x has been extensively examined and discussed in the literature. For such thermal phase transitions, a critical temperature T_{MI} is associated with the change in sign of the slope of $\sigma(T)$ [7]. For example, for $2 \leqslant x < 3$ a thermal transition typically occurs around $T_{MI} \cong 250$ K which is attributed to hydrogen vacancy ordering at octahedral sites, i.e. H atoms 'freeze' in a disordered superstructure [8]. In contrast, we investigate a unique MI transition *as a function of* n for thin-film YH_x *at* $T = 0$ K. For this quantum phase transition, the critical charge carrier density n_c is defined as the value at which the residual conductivity $\sigma(n, T = 0) \equiv \sigma_0(n)$ changes from a finite value in the metallic phase ($n > n_c$) to zero in the insulating phase ($n < n_c$). We determine n both at $T = 0.35$ K, close to the lowest T available to us in a ^{3}He cryostat, and at 15 K, where n can be accurately determined from ρ_{xy}-measurements without the need of ρ_{xx}-compensation which becomes necessary in the insulating phase at low T. The scaling analysis which we present and apply to our $\sigma(n, T)$ data yields the same results using either $n(0.35\ \text{K})$ or $n(15\ \text{K})$. This indicates that n at fixed T is a good tuning parameter, even in the presence of carrier freeze-out [9]. We therefore omit the temperature index for n unless necessary for clarity and in the figure captions for completeness.

The scaling analysis presented here is based on predictions of quantum scaling theory for continuous $T = 0$ MI transitions in the presence of disorder and electron correlations [10]. We use it to determine the static and dynamic critical exponents which characterize the nature of the underlying $T = 0$ MI transition. Values from the scaling analysis in the insulating phase and from collapse of data to a single master curve in the critical region are consistent with values independently found from the scaling analysis in the metallic phase. The present analysis differs from the one applied before [2, 3] in that we include *a priori* n-dependent corrections. This approach extends the region of the (n, T) phase diagram over which data collapse can be found and leads to a straightforward interpretation of the conditions under which it fails. The introduction of corrections to scaling does not affect the value of the critical exponents. The unusually large magnitude of the product of the dynamic and static critical exponents, $z\nu = 6.0 \pm 0.5$, appears to indicate the important role played by electron–electron interactions at the $T = 0$ MI transition of YH_x, in accord with earlier theoretical predictions for the nature of the insulating state of YH_3 [11].

2. Scaling analysis

A continuous quantum phase transition involves a correlation length ξ and a correlation time ξ_τ which diverge as functions of the tuning parameter, i.e. $\xi(n) \propto |n/n_c - 1|^{-\nu}$ and $\xi_\tau(n) \propto |n/n_c - 1|^{-z\nu}$, with ν and z the static and dynamic critical exponents, respectively [4]. At a continuous $T = 0$ MI transition, $\sigma_0(n)$ vanishes continuously to 0 in the metal with power-law dependence on the tuning parameter n:

$$\sigma_0(n) = \sigma_{00}(n/n_c - 1)^{\mu}, \qquad n \downarrow n_c, \tag{1}$$

where μ is the conductivity exponent, and $\sigma_0(n < n_c) \equiv 0$ in the insulating phase. Furthermore, the critical conductivity curve $\sigma(n = n_c, T) \equiv \sigma_c(T)$ is expected to have power-law behaviour as a function of T:

$$\sigma_c(T) = A_c T^{\mu/z\nu}, \qquad n = n_c,\ T \to 0. \tag{2}$$

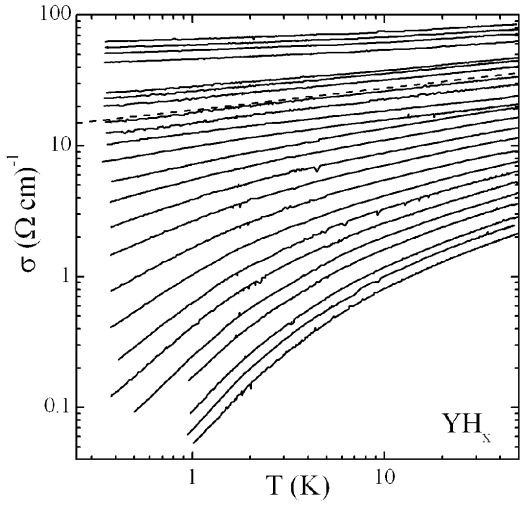

Figure 1. Electrical conductivity σ versus temperature T of a single yttrium hydride thin film, for various values of the charge carrier density n (solid curves). The critical conductivity curve $\sigma_c(T)$ at the $T = 0$ MI transition is shown as a dashed line. From top to bottom: $n(0.35\ \mathrm{K}) = 2.5, 2.32, 2.12, 1.88, 1.64, 1.51, 1.45, 1.18, 1.07, 0.89 \times 10^{19}\ \mathrm{cm}^{-3}$; $n(15\ \mathrm{K}) = 2.04, 1.97, 1.82, 1.65, 1.53, 1.36, 1.24, 1.14, 1.04, 0.94, 0.87, 0.77, 0.73, 0.67 \times 10^{19}\ \mathrm{cm}^{-3}$.

A log–log plot of σ versus T is best suited for an initial identification of such power-law behaviour. The upper seven curves in figure 1 have positive curvature (extrapolating to finite σ_0), while the other curves have negative curvature (extrapolating to $\sigma_0 = 0$); consequently, there must be a zero-curvature line in between (corresponding to power-law behaviour, with $\sigma_0 = 0$). An unusually small power $\mu/z\nu = 1/6$ can be estimated from the slope of the curves in the critical region in figure 1. Indeed, on a linear scale only a plot of σ versus T^p with power $p = 0.167 \pm 0.015$ produces straight lines (figure 2). The initial report of logarithmic temperature behaviour at higher T of the resistivity of thin-film YH_x by Huiberts *et al* [9] is less accurate: power-law behaviour T^p with small power p is easily misinterpreted as $\ln T$ behaviour, since $T^p \overset{p\to 0}{\approx} 1 + p \ln T$ for T not too small. We observe power-law behaviour over at least three decades in T, permitting us to accurately determine $\sigma_0(n)$, n_c, and A_c from extrapolation. To that end, and in accord with equations (1) and (2), we fit

$$\sigma(n, T) = \sigma_0(n) + A_M(n) T^{\mu/z\nu}, \qquad n \downarrow n_c,\ T \to 0 \tag{3}$$

to the various curves in the metallic part of the critical region in figure 2. Here we introduce an n-dependent correction: we do not fix the prefactor to A_c but allow A_M to vary with n, where $A_M(n = n_c) \equiv A_c$.

Instead of a conductivity jump of the order of $\sigma_{Mott} = 30\ \Omega^{-1}\ \mathrm{cm}^{-1}$, which is expected in the case of a discontinuous $T = 0$ MI transition, we find that $\sigma_0(n)$ continuously drops to 0 at $n_c(0.35\ \mathrm{K}) = 1.39 \pm 0.03 \times 10^{19}\ \mathrm{cm}^{-3}$ (see figure 2 inset, right axis) or at $n_c(15\ \mathrm{K}) = 2.8 \pm 0.1 \times 10^{19}\ \mathrm{cm}^{-3}$ (not shown). The occurrence of a simultaneous structural transition can be ruled out, since it would wash out any continuous quantum critical behaviour. This is corroborated by our finding that the transition takes place for $x > 2.86$, i.e. in the purely hcp γ-phase of YH_x. We determine the hydrogen content x for measurements up to RT by comparison of σ (RT) with values obtained in electrolysis experiments [12] and conclude that $2.86 < x_c < 2.93$ (with x_c the critical hydrogen content corresponding to n_c). Moreover, it is unlikely that the formation of an octahedral hydrogen superlattice structure is at the origin of the

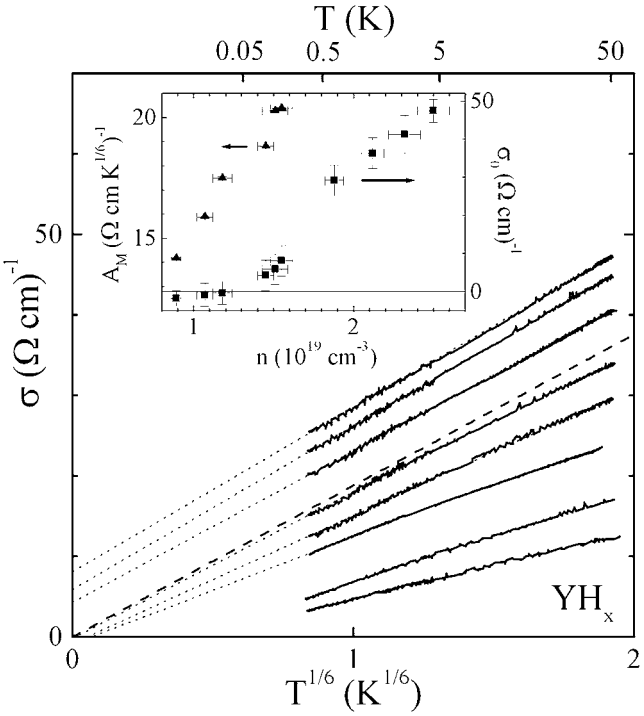

Figure 2. A replot of the data in figure 1 to emphasize the power-law behaviour of the conductivity σ with temperature T (solid lines), expected on the metallic side of the critical conductivity curve $\sigma_c(T)$ (dashed line). Dotted lines are linear fits according to equation (3) in the text. From top to bottom: $n(0.35\ \mathrm{K}) = 1.64, 1.51, 1.45, 1.18, 1.07, 0.89, 0.75, 0.5 \times 10^{19}\ \mathrm{cm}^{-3}$. Inset: The residual conductivity σ_0 (squares, right axis) and prefactors A_M (triangles, left axis) as a function of the charge carrier density n at $T = 0.35$ K. They are determined as the abscissa and slope, respectively, of the fits in the main figure.

$T = 0$ MI transition since seven such structures are theoretically predicted and experimentally identified [8], while only one $T = 0$ MI transition is observed. However, hydrogen vacancy ordering could be responsible for PPC and play a role in charge carrier doping, similar to the role that oxygen vacancy ordering plays for PPC in the high-T_c superconductor $YBa_2Cu_3O_{7-\delta}$ [13]. We emphasize that PPC also exists in the metallic phase and the $T = 0$ MI transition can be traversed using PPC alone (e.g. curves 5–10 from above in figure 1).

With n_c identified, $A_c \equiv A_M(n = n_c) = 18.8 \pm 0.3\ \Omega^{-1}\ \mathrm{cm}^{-1}\ \mathrm{K}^{-1/6}$ is determined simply from $A_M(n)$ (see figure 2 inset, left axis). The critical conductivity curve $\sigma_c(T)$ is then specified. The conductivity exponent μ can be identified from the slope of σ_0 versus $(n-n_c)/n_c$ according to equation (1). We find $\mu = 1.0 \pm 0.1$ (see figure 4, right axis), giving $z\nu = 6.0 \pm 1.1$. This value is much higher than the $z\nu = 2$ which has been derived from scaling analyses of the amorphous alloy NbSi [14] and the doped semiconductor Si:P [15], where the MI transition is governed mainly by disorder (Anderson limit). It is only comparable to $z\nu = 4.6 \pm 0.4$ found for the Mott–Hubbard transition metal compound $NiS_{2-x}Se_x$ [16], where a large value of $z\nu$ seems to mark a continuous MI transition in the highly correlated limit. Theoretically it has been shown [11] that the formation of an inverted Zhang–Rice singlet (i.e. the hybridization of a 1s H orbital with an almost empty 4d Y orbital) can lead to the observed 3 eV optical gap of YH_3. It still remains an open question whether the corresponding effective Hamiltonian also produces the large critical exponent values observed here.

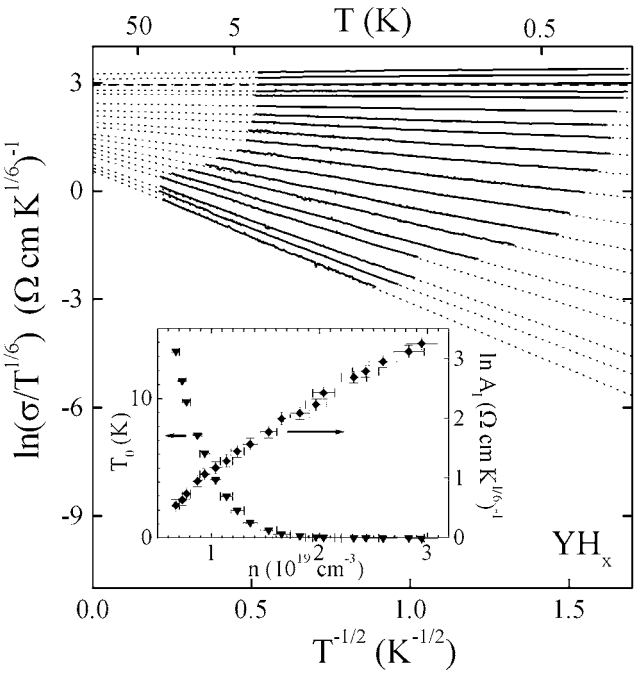

Figure 3. A replot of the data in figure 1 to single out the exponential behaviour of $\sigma(T)$ (solid lines), expected on the insulating side of the critical conductivity curve $\sigma_c(T)$ (dashed line). Dotted lines are linear fits according to equation (4) in the text. From top to bottom: $n(15\ \mathrm{K}) = 2.95$, 2.83, 2.59, 2.43, 2.32, 2.04, 1.97, 1.82, 1.65, 1.53, 1.36, 1.24, 1.14, 1.04, 0.94, 0.87, 0.77, 0.73, 0.67×10^{19} cm^{-3}. Inset: the Coulomb gap temperature T_0 (triangles, left axis) and the natural logarithm of the prefactors A_I (diamonds, right axis) as a function of the charge carrier density n at $T = 15$ K. They are determined as the slope and abscissa, respectively, of the fits in the main figure.

In order to describe our data on the insulator, we account for thermal activation over a Coulomb gap via [14, 15]

$$\sigma(n, T) = A_I(n) T^{\mu/z\nu} \exp -(T_0(n)/T)^{\beta}, \qquad n \uparrow n_c,\ T \to 0 \tag{4}$$

where $k_B T_0$ is the Coulomb gap energy with $T_0(n > n_c) \equiv 0$. Again, we introduce an n-dependent correction: we do not fix the prefactor to A_c but explicitly allow A_I to vary with n, where $A_I(n = n_c) \equiv A_c$. With $\mu/z\nu = 1/6$ found above, β is determined by plotting $\ln(\sigma/T^{1/6})$ versus $T^{-\beta}$ for various values of β and looking for linear behaviour, as is expected from equation (4). Only for $\beta = 0.50 \pm 0.02$ do we find such linear behaviour over an extended T-interval (see figure 3). This value is predicted for Efros–Shklovskii hopping transport in the case of a soft Coulomb gap due to electron–electron interactions, another indication of the dominant role of strong correlations at the $T = 0$ MI transition of YH_x.

With β known, $A_I(n)$ can be determined from the abscissa in figure 3 and we find $A_c \equiv A_I(n_c) = 20.0 \pm 1.0\ \Omega^{-1}\ \mathrm{cm}^{-1}\ \mathrm{K}^{-1/6}$ (see figure 3 inset, right axis). The Coulomb gap temperature $T_0(n)$ can now be determined from the slope of the curves in figure 3 (see figure 3 inset, left axis): it drops continuously to zero at $n_c(15\ \mathrm{K}) = 2.8 \pm 0.1 \times 10^{19}$ cm^{-3}. The Coulomb gap energy is related to the dielectric constant κ and the correlation length ξ by $k_B T_0 = (2.8e^2/4\pi\varepsilon_0)(\kappa\xi)^{-1}$ [17]. Consequently,

$$T_0(n) = T_{00}(1 - n/n_c)^{z\nu}, \qquad n \uparrow n_c, \tag{5}$$

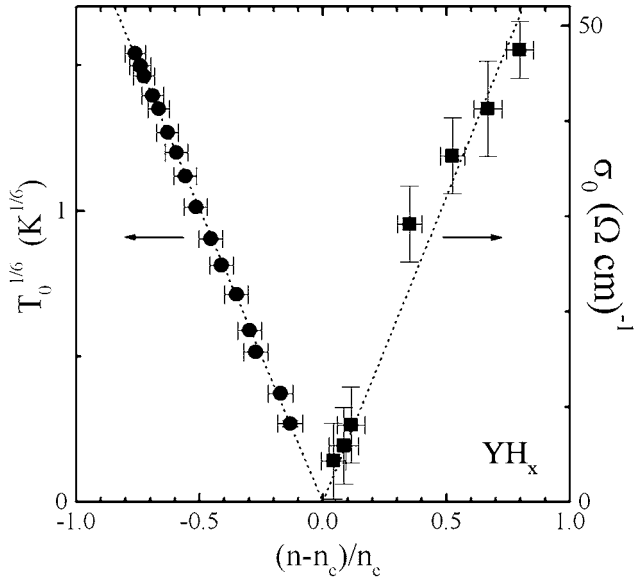

Figure 4. Residual conductivity σ_0 (squares, right axis) and Coulomb gap temperature $T_0^{1/6}$ (circles, left axis) as a function of the distance to the quantum critical point, $n - n_c$. Dotted lines are linear fits to the σ_0- and $T_0^{1/6}$-data according to equations (1) and (5) in the text, respectively.

with $\kappa(n) \propto (1 - n/n_c)^{-(z-1)\nu}$. The product $z\nu$ of the dynamic and static critical exponents can be determined from the slope of T_0 versus $(1 - n/n_c)$ on a log–log plot, yielding $z\nu = 6.0 \pm 0.1$ (figure 4, left axis). The values of n_c(15 K), A_c, and $z\nu$ found by these fits for the insulator are consistent with the ones previously determined independently for the metal, confirming the validity of our analysis.

Finally, we regard the prediction by quantum scaling theory of data collapse onto a universal curve for $n \to n_c$:

$$\sigma/\sigma_c = \mathcal{F}_M([n - n_c]/n_c T^{1/z\nu}), \qquad n \downarrow n_c,\ T \to 0, \tag{6a}$$

$$\sigma/\sigma_c = \mathcal{F}_I([n_c - n]/n_c T^{1/z\nu}), \qquad n \uparrow n_c,\ T \to 0, \tag{6b}$$

i.e. on the metallic (insulating) side of the critical point all $\sigma(n, T)$ curves, normalized to the critical conductivity curve, can be described by a single function $\mathcal{F}_M$ ($\mathcal{F}_I$), which is dependent *solely* on the scaling variable $|n - n_c|/n_c T^{1/z\nu}$. However, by not fixing the prefactors A_M and A_I to A_c (in equations (3) and (4)) and allowing them to vary with n, we also introduce n-dependent corrections to data collapse. This becomes apparent when explicitly rewriting equations (3) and (4) (using equations (1), (2) and (5)) as

$$\sigma/\sigma_c = (\sigma_{00}/A_c)([n - n_c]/n_c T^{1/z\nu})^{\mu} + A_M(n)/A_c, \qquad n \downarrow n_c,\ T \to 0, \tag{7a}$$

$$\sigma/\sigma_c = (A_I(n)/A_c)\exp -T_{00}^{\beta}([n_c - n]/n_c T^{1/z\nu})^{\beta z\nu} \qquad n \uparrow n_c,\ T \to 0. \tag{7b}$$

When comparing equations (6) and (7), it is clear that we add a correction term $(1 - A_M(n)/A_c)$ to the left-hand side of equation (6*a*), while the left-hand side of equation (6*b*) is multiplied by a correction factor $A_c/A_I(n)$.

Fixing n_c to the previously found values and allowing $z\nu$ to vary, data collapse according to equation (6*a*) is indeed observed for $z\nu = 6.0 \pm 0.5$ (see figure 5, left axis) in the (n, T) range of the metallic phase that we experimentally probe, i.e. $0.04 < n/n_c - 1 < 0.8$ and $0.3\ \text{K} < T < 50\ \text{K}$. In the absence of a quantitative calculation of the range of the critical

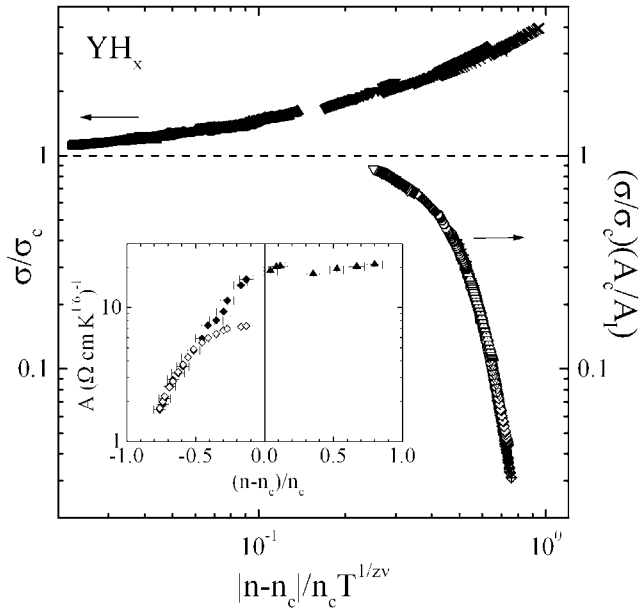

Figure 5. Collapse of the conductivity data $\sigma(n, T)$ from figure 1 onto a universal curve. For the metal, $\sigma(n, T)$ is normalized to the critical conductivity curve $\sigma_c(T)$ (filled symbols, left axis) and plotted as a function of the scaling parameter $|n - n_c|/n_c T^{1/z\nu}$, according to equation (6*a*). Here ν and z are the static and dynamic critical exponents, respectively. To invoke data collapse for the insulator, the normalized data have to be multiplied by a correction factor as described in the text (open symbols, right axis). Inset: the prefactors $A_M(n)$ of the metallic curves (upward-pointing triangles) and $A_I(n)$ of the insulating curves (closed diamonds) as a function of the distance to the quantum critical point. The open diamonds represent $A_I(n)$ according to equation (8) in the text. This description fails for $1 - n/n_c < 0.5$.

region and without a theoretical criterion for true overlap of data, we tentatively estimate the extent of the critical region in the metallic phase from the observed data collapse. For $n/n_c - 1 < 0.1$ the critical region ranges at least from $T = 50$ K down to 0.3 K, while for $0.4 < n/n_c - 1 < 0.8$ it only reaches down to approximately 10 K: deviations from a single master curve clearly appear at low T for n further from n_c (see figure 5, metal). Application of the correction term does not lead to a change of these results, as expected from the weak variation of $A_M(n)$ for $n \downarrow 0$ (see figure 5 inset).

By contrast, data collapse according to equation (6*b*) is not observed for any $z\nu$ in the (n, T) range of the insulating phase that we probe, i.e. $0.13 < 1 - n/n_c < 0.8$ and $0.3\ \text{K} < T < 50$ K—although this includes a range of values of $|n/n_c - 1|$ and T where data collapse does exist for the metal. Only application of the correction factor leads to data collapse, again for $z\nu = 6.0 \pm 0.5$ (see figure 5, insulator), now for $1 - n/n_c < 0.8$ but at temperatures from approximately 20 K down to at least 0.3 K. This is in contrast to the n-dependent correction *a posteriori* introduced in [3], which invokes data collapse in the same temperature range, but only for $0.5 < 1 - n/n_c < 0.8$. There we noted that the $\ln(\sigma/T^{1/6})$ versus $T^{-1/2}$ curves with $T_0(n) > 0.55$ K intersect in a single point, implying that $A_I(n)$ for these curves is well described by

$$A_I(n) = A_c \exp -(1 + \alpha T_0^{\beta}(n)), \tag{8}$$

with $\alpha = 0.39$. However, this description fails for curves with $T_0(n) < 0.55$ K (see the inset in figure 5). The present analysis leads to a straightforward interpretation of the observed failure of universal scaling in the absence of corrections, but at the cost of obscuring the simple form of the corrections to scaling given by equation (8): the need for large, almost exponentially varying corrections $A_I(n)$ (see figure 5 inset) indicates that the insulating side of the critical region has a smaller extent than its metallic counterpart. We predict collapse onto a universal curve without corrections to occur for the insulator for $|n/n_c - 1| \ll 0.13$, while for the metal we expect that it should extend beyond $|n/n_c - 1| > 0.8$, ranges which are not covered by our present experiments.

We conclude by emphasizing that a consistent value for $z\nu$ is found via all the methods discussed above. Furthermore, when comparing the values of $z\nu$, n_c, and A_c to those determined in the analyses of [2] and [3], we find, as we should, that they are unaffected by the *a priori* introduction of n-dependent corrections.

3. Summary

In summary, we determine $\sigma(n, T)$ of a single YH_x thin film while driving it through the $T = 0$ MI transition using hydrogenation at RT and PPC at low T. Values of the conductivity exponent μ and the product of the dynamic and static exponents $z\nu$ are determined from a scaling analysis. On the insulating side of the quantum critical point we find $z\nu = 6.0 \pm 0.1$, consistent with $z\nu = 6.0 \pm 1.1$ and $\mu = 1.0 \pm 0.1$ independently determined on the metallic side. Collapse of the data onto a master curve is observed for our data in the metal for $z\nu = 6.0 \pm 0.5$. However, n-dependent corrections have to be introduced to invoke data collapse for the insulator, again for $z\nu = 6.0 \pm 0.5$. Since the insulating data set covers a range of the (n, T) phase diagram equivalent to that for the metallic data, this indicates that the critical region extends further on the metallic than on the insulating side. The agreement between the values of $z\nu$ determined in various ways validates the proposed scaling analysis. The large value of $z\nu$ appears to indicate the important role played by electron–electron interactions in the physics of the switchable mirrors.

Acknowledgments

We are grateful to R Griessen for his continuing interest and scientific cooperation. This work was supported by the Royal Netherlands Academy of Arts and Sciences, the Dutch Stichting voor Fundamenteel Onderzoek der Materie and by the National Science Foundation under Grant DMR-0114798.

References

[1] Huiberts J N *et al* 1996 *Nature* **380** 231
[2] Hoekstra A F Th *et al* 2001 *Phys. Rev. Lett.* **86** 5349
[3] Roy A S *et al* 2002 *Phys. Rev. Lett.* **89** 276402
[4] Sondhi S L *et al* 1997 *Rev. Mod. Phys.* **69** 315
[5] Voss D 2001 *Science* **292** 1987
[6] Hoekstra A F Th, Rosenbaum T F and Roy A S 2002 *Rev. Sci. Instrum.* **73** 119
[7] Shinar J *et al* 1988 *Phys. Rev.* B **37** 2066
Daou J N and Vajda P 1992 *Phys. Rev.* B **45** 109071
[8] Sun S N, Wang Y and Chou M Y 1994 *Phys. Rev.* B **49** 648
Kai K *et al* 1989 *Phys. Rev.* B **40** 6591
[9] Huiberts J N *et al* 1997 *Phys. Rev. Lett.* **79** 3724

[10] Lee P and Ramakrishnan T V 1985 *Rev. Mod. Phys.* **57** 287
Altshuler B L and Aronov A G 1985 *Electron–Electron Interactions in Disordered Systems* ed A L Efros and M Pollak (New York: Elsevier)
[11] Ng K K *et al* 1997 *Phys. Rev. Lett.* **78** 1311
Eder R, Pen H F and Sawatzky G 1997 *Phys. Rev.* B **56** 10115
van Gelderen P *et al* 2000 *Phys. Rev. Lett.* **85** 2989
[12] Kooij E S, van Gogh A T M and Griessen R 1999 *J. Electrochem. Soc.* **146** 2990
[13] Kudinov V I *et al* 1993 *Phys. Rev.* B **47** 9017
Kawamoto K and Hirabayashi I 1994 *Phys. Rev.* B **49** 3655
[14] Lee H-L *et al* 2000 *Science* **287** 633
[15] Bogdanovich S, Sarachik M P and Bhatt R N 1999 *Phys. Rev. Lett.* **82** 137
[16] Husmann A *et al* 1996 *Science* **274** 1874
Husmann A *et al* 2000 *Phys. Rev. Lett.* **84** 2465
[17] McMillan W L 1981 *Phys. Rev.* B **24** 2739
Watanabe M *et al* 1998 *Phys. Rev.* B **58** 9851